Kobe University Repository : Kernel

PDF issue: 2025-12-05

Forming-free resistive switching in solution-processed silicon nanocrystal thin film

Kawauchi, Takeshi

Kano, Shinya

Fujii, Minoru

(Citation)
Journal of Applied Physics,124(8):085113-085113

(Issue Date)
2018-08-28

(Resource Type)
journal article

(Version)
Version of Record

(Rights)
©2018 AIP Publishing. This article may be downloaded for personal use only. Any other use requires prior permission of the author and AIP Publishing. The following article appeared in Journal of Applied Physics 124(8), 085113 and may be found at http://dx.doi.org/10.1063/1.5032244

(URL)
https://hdl.handle.net/20.500.14094/90005232

KOBE UNIVERSITY

Forming-free resistive switching in solution-processed silicon nanocrystal thin film

Takeshi Kawauchi, Shinya Kano, and Minoru Fujii

Citation: Journal of Applied Physics **124**, 085113 (2018); doi: 10.1063/1.5032244
View online: https://doi.org/10.1063/1.5032244
View Table of Contents: http://aip.scitation.org/toc/jap/124/8
Published by the American Institute of Physics

Articles you may be interested in

Estimating complete band diagrams of non-ideal heterointerfaces by combining ellipsometry and photoemission spectroscopy
Journal of Applied Physics **124**, 085302 (2018); 10.1063/1.5034774

Resistive switching study in HfO_2 based resistive memories by conductive atomic force microscopy in vacuum
Journal of Applied Physics **124**, 014501 (2018); 10.1063/1.5025143

Controlling the thin interfacial buffer layer for improving the reliability of the Ta/Ta_2O_5/Pt resistive switching memory
Applied Physics Letters **113**, 072902 (2018); 10.1063/1.5040430

Tutorial: Organic field-effect transistors: Materials, structure and operation
Journal of Applied Physics **124**, 071101 (2018); 10.1063/1.5042255

Model of dielectric breakdown in hafnia-based ferroelectric capacitors
Journal of Applied Physics **124**, 024103 (2018); 10.1063/1.5031491

Topological insulator-metal transition and molecular electronics device based on zigzag phagraphene nanoribbon
Journal of Applied Physics **124**, 084303 (2018); 10.1063/1.5029845

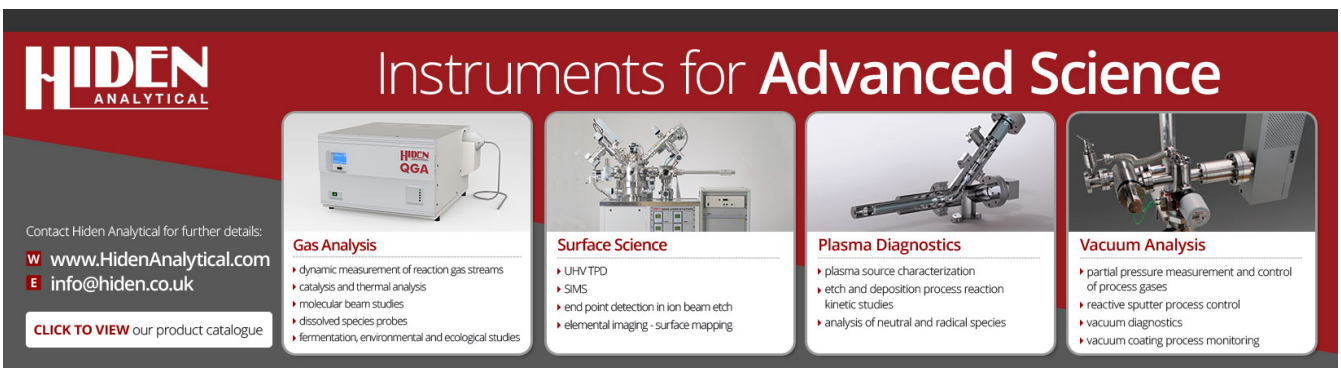

Forming-free resistive switching in solution-processed silicon nanocrystal thin film

Takeshi Kawauchi, Shinya Kano,[a] and Minoru Fujii
Department of Electrical and Electronic Engineering, Graduate School of Engineering, Kobe University, Kobe 657-8501, Japan

(Received 3 April 2018; accepted 10 August 2018; published online 28 August 2018)

We report a forming-free resistive switching using a solution-processed silicon nanocrystal (Si NC) thin film. A Si NC thin film is formed on an ITO/glass substrate by spin-coating a colloidal Si NC solution in air. The Si NC thin film shows bipolar resistive switching without a forming process. Electrical characteristics at low temperatures and in various gas environments suggest that a non-stoichiometric SiO_x shell on Si NCs contributes to the resistive switching. We propose that the origin of the resistive switching is a conductive filament of oxygen vacancies on the SiO_x shell by an electric field. *Published by AIP Publishing.* https://doi.org/10.1063/1.5032244

I. INTRODUCTION

Resistive switching has attracted great attention because of its potential application in resistive random access memories (ReRAMs).[1–4] Resistive switching memories have a metal-insulator-metal structure. A conductive filament made from metal atoms or oxygen vacancies is formed or destructed by an applied voltage in the insulator. This atomic rearrangement results in resistive switching. In order to make a conductive filament in the insulator, a forming process is usually required to breakdown the insulator by a high electric field. Once the forming process is correctly carried out, the insulator is in a soft breakdown condition and its resistance switches reproducibly between a high resistive state (HRS) and a low resistive state (LRS). However, the forming process is a technological issue for the development of resistive switching memories. Several materials showing forming-free resistive switching have been proposed: they contain seeds of a conductive filament in the insulator, such as Pt dispersed in SiO_2[5] and Zn doped in SiO_x.[6]

Recently, solution-processed nanoparticle (NP) or nanocrystal (NC) thin films are considered as insulator layers in resistive switching memories.[7–13] One advantage of these films is a vacuum-free solution process. Because the vacuum-free solution process is suitable for deposition of colloidal NPs or NCs on organic or polymer substrates, flexible resistive switching memories can be produced.[8,9] Kim *et al.* reported resistive switching in an insulator layer made of Fe_3O_4 NPs (7, 9, 12, and 15 nm in diameter).[10] Kim *et al.* found that resistive switching occurred in a composite of alkendienyl passivated Si NPs (4–6 nm in diameter) and polystyrene polymers.[11] Similar resistive switching has been reported in the NP thin films made of ZnO NPs[12] and Ni-Au NPs.[13]

Si-based resistive switching memory is also potentially promising because Si is environmentally friendly, naturally abundant, and CMOS compatible. Yao *et al.* reported a high ON/OFF ratio ($>10^5$), a fast switching (sub-100 ns), and good endurance (10^4 switching cycles) in a resistive switching memory with a SiO_x ($x \leq 2$) insulating layer.[14] They attributed the resistive switching to the formation and destruction of a conductive filament of Si NCs in a SiO_x insulator. On the other hand, Mehonic *et al.* explained the resistive switching in a SiO_x film by the formation and destruction of a conductive filament of oxygen vacancies.[15–19] In these previous research studies, Si oxide films are produced by a vacuum process.

In this work, we combine the following ideas: forming-free resistive switching, a vacuum-free solution process, and a Si-based resistive memory. We focus on a solution-processed film containing Si oxides for forming-free resistive switching. For obtaining forming-free resistive switching, we adopt the colloidal solution of Si NCs codoped with B and P.[20–22] Electronic and optoelectronic device applications of colloidal Si NC solution have been intensively studied.[23–25] In our previous work, a flat Si NC thin film (≈50 nm thickness, formed by spin-coating the colloidal Si NC solution) was highly resistive at low voltage because non-stoichiometric amorphous SiO_x at the surface of Si NCs acted as tunneling barriers.[22] We conceive that this SiO_x at the surface of Si NCs can be used as a resistive switching layer. For the proof of concept, we demonstrate that a Si NC thin film sandwiched by aluminum (Al) and indium-tin-oxide (ITO) electrodes shows a reproducible resistive switching without a forming process. We also propose that oxygen vacancies in non-stoichiometric amorphous SiO_x at the surface of Si NCs are a reasonable origin of resistive switching.

II. EXPERIMENTAL

B and P codoped Si NCs were prepared by a co-sputtering method described in our previous papers.[21,26,27] Si-rich borophosphosilicate glass (BPSG) films were deposited on a thin stainless steel plate (thickness: 0.1 mm) by co-sputtering Si, SiO_2, B_2O_3, and P_2O_5. We collected the films by bending the plate and the films were crushed in a mortar. The powder was annealed in a nitrogen (N_2) atmosphere at 1100 °C for 30 min to grow Si NCs in a BPSG matrix. The annealed powder was dissolved in a hydrofluoric acid (HF)

[a]Author to whom correspondence should be addressed: kano@eedept.kobe-u.ac.jp

solution (46 wt. %) for 30 min in an ultrasonic bath to extract Si NCs from the matrix. Si NCs were separated from the HF solution by centrifugation (4000 rpm, 1 min) in a centrifugal concentrator (Sartorious, VIVASPIN 2, 10,000 MWCO PES). Methanol was then added to the centrifugal concentrator in order to transfer Si NCs from HF to methanol. The centrifugation was repeated several times. In this study, Si NCs were stored in methanol for more than 30 days in ambient air. During the storage, surface oxides were formed on NCs. The concentration of Si NCs in methanol was 0.5 mg/ml. It should be noted that the codoped Si NCs are completely dispersed in methanol without organic ligands because of negative surface potential: this is different from other reported colloidal Si NCs and NPs capped with organic ligands.[26] A flat and dense film can be prepared on an arbitrary substrate by spin-coating the solution.[22,28,29]

Figure 1(a) shows a photograph of a colloidal Si NC solution. The solution is very clear due to perfect dispersion of codoped Si NCs in methanol. Figure 1(b) shows a transmission electron microscopy (TEM) image of Si NCs (JEOL, JEM-200CX). The average diameter (D_{ave}) is 4.9 nm with the standard deviation of 1.1 nm (Fig. S1 in the supplementary material). The lattice fringe in the high-resolution TEM (HRTEM) image (inset) corresponds to {111} planes of the Si crystal.[27] Fig. 1(c) shows an infrared (IR) absorption spectrum of a Si NC thin film on a Au-coated Si substrate (PerkinElmer, Spectrum GX). A major peak around 1065 cm^{-1} is assigned to the Si-O-Si asymmetric stretching mode. On the other hand, the Si-H stretching mode at 2100–2200 cm^{-1} is not clearly observed. Therefore, the surface of Si NCs is mainly terminated by native Si oxides. Figure 1(d) shows a Si 2p X-ray photoelectron spectroscopy (XPS) spectrum of a Si NC thin film on a Au-coated Si substrate (ULVAC-PHI, PHI X-tool). The signal is composed of five oxidation states of Si: Si^0 (99.8 eV), Si^{1+} (100.7 eV), Si^{2+} (101.5 eV), Si^{3+} (102.5 eV), and Si^{4+} (103.5 eV).[30] The signals of Si^0 and Si^{4+} arise from Si NC cores [observed in the inset of Fig. 1(b)] and surface oxides on Si NCs, respectively.[31] The observation of Si^{1+}, Si^{2+}, and Si^{3+} signals suggests that the surface is not completely oxidized. In other words, the surface oxides are not SiO_2 but non-stoichiometric SiO_x and have oxygen vacancies. The codoped Si NC consists of crystalline Si (core) and non-stoichiometric amorphous SiO_x at the surface of Si NCs (shell), as schematically shown in the inset. It is noted that stoichiometric SiO_2 does not show a resistive switching.[6] Figure 1(e) shows an atomic force microscopy (AFM) (SII, SPA400) topographic image of a solution-processed Si NC thin film.[32] A histogram of the height in the AFM image is shown in the supplementary material (Fig. S2). The root-mean-square (RMS) of the surface roughness is 1.5 nm in the 1 × 1 μm^2 area.

Figure 1(f) shows a schematic device structure studied in this work. Following the cleaning of an ITO (90 nm)/glass substrate by ultrasonication in acetone and isopropyl alcohol (IPA) and by UV/O_3 treatments, a drop of a colloidal Si NC solution was spin-coated and dried on the substrate at room temperature in air. The thickness of the film was 41 nm, which was obtained from the absorbance of a Si NC thin film on a silica substrate. We had an absorption coefficient of a Si NC film and calculated the thickness from the absorbance of 350 nm wavelength. The detailed method is shown in the supplementary material. Circular Al electrodes (diameter: 1 mm and thickness: 55 nm) were deposited by thermal evaporation. Tan *et al.* proposed that native Al oxides were formed at the CeO_{2-x}/Al interface, which contributed to a resistive switching behavior. In our study, because a contact between Al and Si NCs was formed under vacuum by thermal evaporation, no native Al oxides were formed at the Al/Si NC interface.[33,34] Current-voltage characteristics were measured by a source measure unit (Keithley, 236). Measurements were

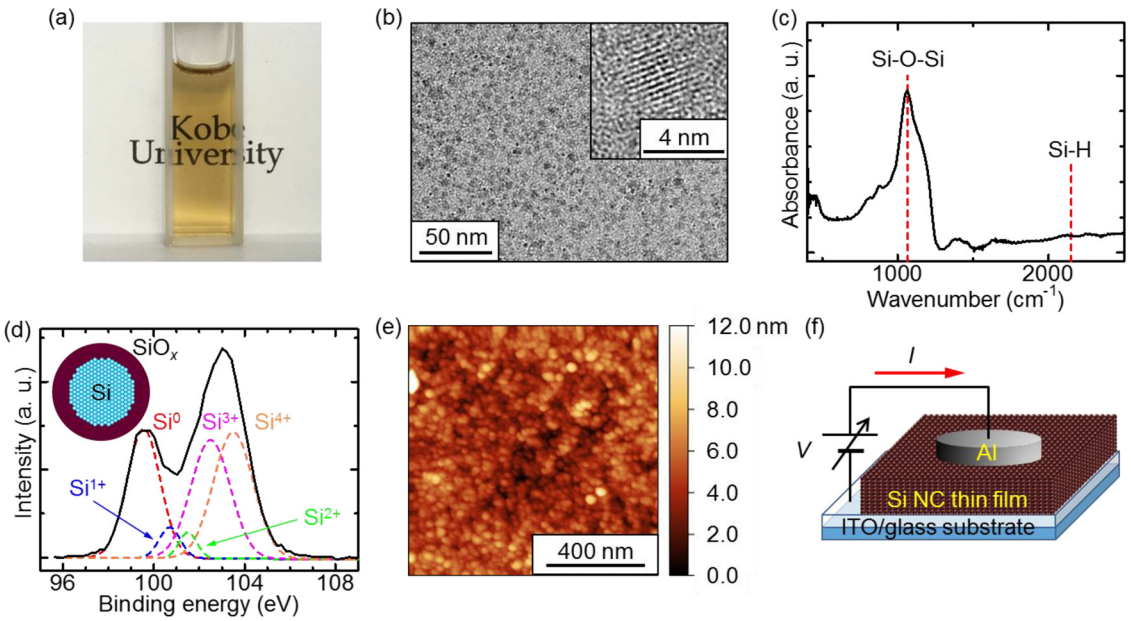

FIG. 1. (a) Photograph of colloidal Si NC solution in methanol. (b) TEM image of Si NCs grown at 1100 °C. The inset shows a HRTEM image of a single Si NC. (c) IR absorption spectrum of a Si NC thin film. (d) XPS spectrum of a Si NC thin film. The inset shows a model structure of a Si NC. (e) AFM topographic image of a Si NC thin film. (f) Schematic device structure.

mainly carried out in a cryostat (IWATANI PLANTEC, CRT-007-PL) in vacuum (1.4×10^{-2} mbar). To evaluate environmental dependence, we also measured a device in nitrogen and oxygen gas. When electrical measurements were performed in the cryostat, the Al and ITO electrodes of the samples were mounted on a pin header socket with Au wires using a high conductive silver paste. The socket was set in the cryostat which connected to the source measure unit via BNC cables. In Figs. 2(a), 2(b), and 2(d), we used a probe station (Riko International LTD., *i*E-LN) in vacuum (1.4×10^{-2} mbar) at different temperatures (300–80 K). When electrical measurements were performed in the probe station, tungsten probes were contacted on the ITO and the Al electrodes covered with a silver paste. A positive bias was applied to the Al top electrode in all measurements. A function generator (NF, WF1947), a current-voltage amplifier (Keithley, 428), and an oscilloscope (Iwatsu, DS-5634-A) were used in pulse sequence measurements.

III. RESULTS AND DISCUSSION

We confirm that a solution-processed Si NC thin film has potential as a resistive switching layer as follows. Figure 2(a) shows typical current-voltage characteristics of a solution-processed Si NC thin film. In order to prevent an irreversible breakdown (hard breakdown), we set a current conpliance to 1 μA. The resistance of the Si NC film is 1.4 GΩ at 1 V. When the bias is ramped to the first set voltage (V_{FSet} = 2.6 V), the current suddenly increases and the resistance changes from HRS to LRS (black line). The resistance of LRS is 2.0 MΩ at 1 V. When the bias is ramped over the reset voltage (V_{Reset} = –0.5 V), the current gradually decreases because the resistance changes from LRS to HRS (red line). When the bias is ramped to the set voltage (V_{Set} = 2.8 V) again, the resistance also changes from HRS to LRS (blue line). As a result, a hysteresis appears in the current-voltage characteristics. The ON/OFF ratio at 1 V is 700. It should be noted that V_{FSet} and V_{Set} are similar values, which indicates that the Si NC thin film shows a forming-free resistive switching: a high voltage is not required to obtain a resistive switching.

Set and reset voltages of the same film in several switching cycles are plotted in Fig. 2(b). Set and reset voltages are stable in the switching cycles. Figure 2(c) shows cumulative probability of set and reset voltages in several films. The averages (standard deviation) of set and reset voltages are 2.5 (0.47) V and –1.5 (0.52) V, respectively.

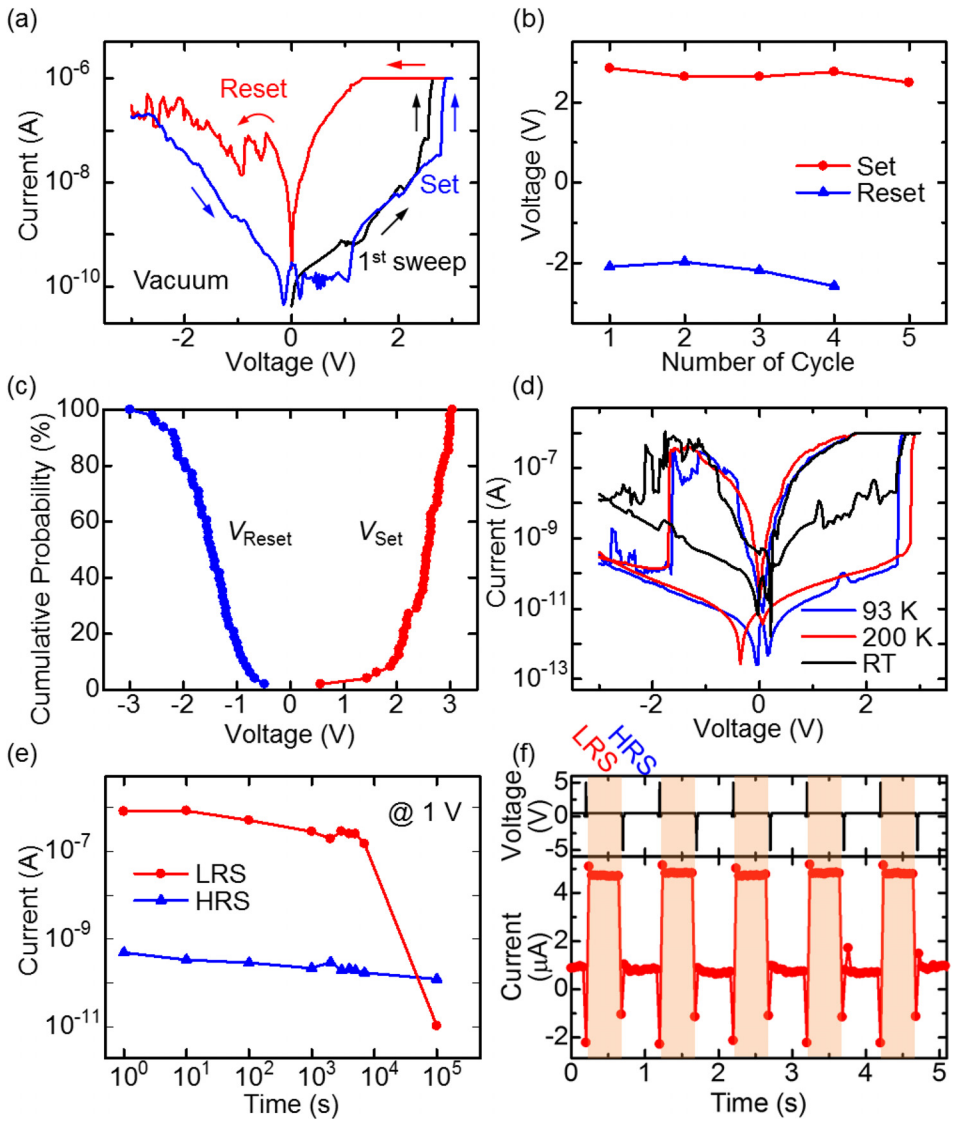

FIG. 2. (a) Typical current-voltage characteristics of a solution-processed Si NC thin film. (b) Set and reset voltages of the same Si NC thin film in several switching cycles. (c) Cumulative probability of set and reset voltages. (d) Temperature dependence of current-voltage characteristics. (e) Retention time at a reading voltage of 1 V. (f) Switching cycles using programmed pulse voltages.

Figure 2(d) shows the temperature dependence of the current-voltage characteristics. The current in HRS decreases by 2 orders of magnitude at low temperature (93 and 200 K), which results in the increase in the ON/OFF ratio to 7000 at 1 V. Set and reset voltages do not depend on the temperatures, which indicates that the switching is induced by an electric field, not by joule heating generated by current.

Figure 2(e) shows the retention time of the resistive switching. To read the current, 1 V is applied as a read voltage. LRS is stable for 7000 s and the state returns to HRS in 10^5 s. On the other hand, HRS is stable for more than 10^5 s. Figure 2(f) shows the switching cycles obtained by using programmed pulse voltages. The programmed pulses consist of set (5 V for 1 ms), reset (–5 V for 5 ms), and read pulses (0.5 V for 460 ms). The resistance of the Si NC thin film is correctly switched by the pulse sequence.

Two major mechanisms are usually considered for resistive switching induced by an electric field.[1] One is the diffusion of an electrochemically active metal from an electrode into an insulator, such as silver and copper.[4,35,36] The other is the migration of oxygen vacancies in an insulator towards the cathode.[15] Since Al and ITO are not electrochemically active, oxygen vacancies in non-stoichiometric SiO_x are reasonable as the origin of the resistive switching. When a positive bias is applied to the top electrode, the oxygen ions with –2 charges are released from a non-stoichiometric amorphous SiO_x shell and are drawn to the top electrode by an electric field. As a result, the filament of oxygen vacancies is formed in a non-stoichiometric amorphous SiO_x shell on the NC surface and the resistance changes from HRS to LRS. The schematic will be shown later.

In Fig. 3, we measure the current-voltage characteristics of the same Si NC thin film in various atmospheres consecutively. The measurement starts in vacuum ($\sim 1 \times 10^{-4}$ mbar), and a resistive switching is observed (top figure). The hysteresis disappears in pure O_2 (1 atm) (2nd figure from the top). It reappears in N_2 (1 atm) (3rd figure from the top) and is the same as that in vacuum (bottom figure). The O_2 molecules degrade the resistive switching. It is noted again that two major mechanisms are usually considered for resistive switching induced by an electric field: filament formation of metal atoms and oxygen vacancies. In the oxygen environment, oxygen vacancies are filled with oxygen gas molecules on a surface of Si NCs and a conductive filament is destructed. Therefore, we adopt that the filament of oxygen vacancies is responsible for the switching.

To further confirm the oxygen vacancy filament model, we oxidize a solution-processed Si NC film in air (annealed at 400 °C for 30 min) and measure the current-voltage characteristics. IR absorption spectra in the left inset show that oxidation proceeds by annealing. The signals of Si^{1+}, Si^{2+}, and Si^{3+} decrease in the XPS spectrum (in the right inset of Fig. 4 and Fig. S3 in the supplementary material) by annealing. In the current-voltage characteristics in Fig. 4, no clear hysteresis is observed after the oxidation. These results indicate that oxygen vacancies on the surface of Si NCs are filled with oxygen ions by annealing in air. Because oxygen vacancies are compensated, the switching does not appear.

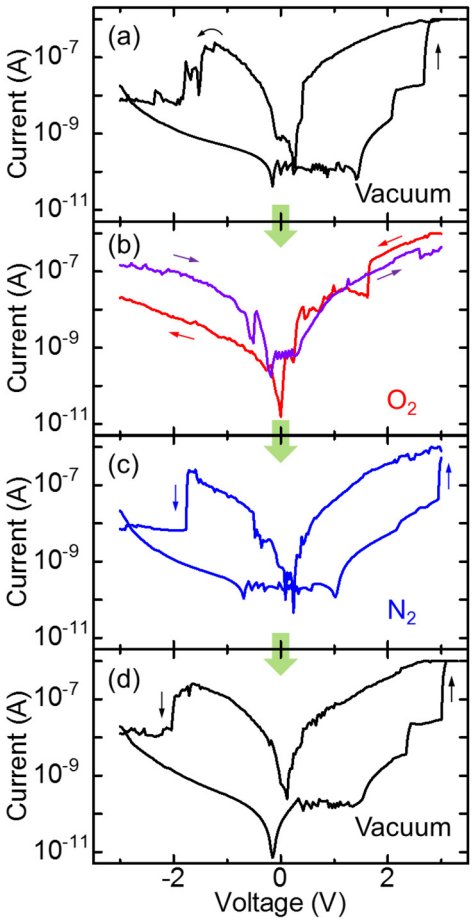

FIG. 3. Current-voltage characteristics of a solution-processed Si NC thin film in various atmospheres.

Figure 5(a) shows a double logarithmic plot of typical current-voltage characteristics. In LRS, the slope is 2.0–2.1, which indicates that the space charge limited current dominates the transport.[37] This suggests that the oxygen vacancy conductive filament does not fully connect between the Al and ITO electrodes and the filament is only partially formed. This partial filament works as a trap of charge carriers and space charge limited condition appears in the conduction of

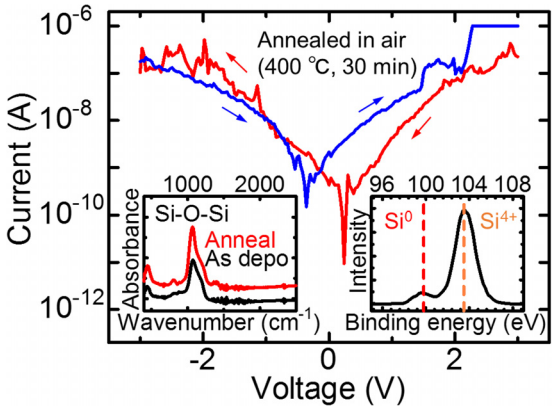

FIG. 4. Current-voltage characteristics of an Al/annealed Si NC thin film/ITO/glass sample. The left inset shows the IR absorption spectra of as-deposited and annealed Si NC thin films. The right inset shows the Si 2p XPS spectrum of an annealed Si NC thin film.

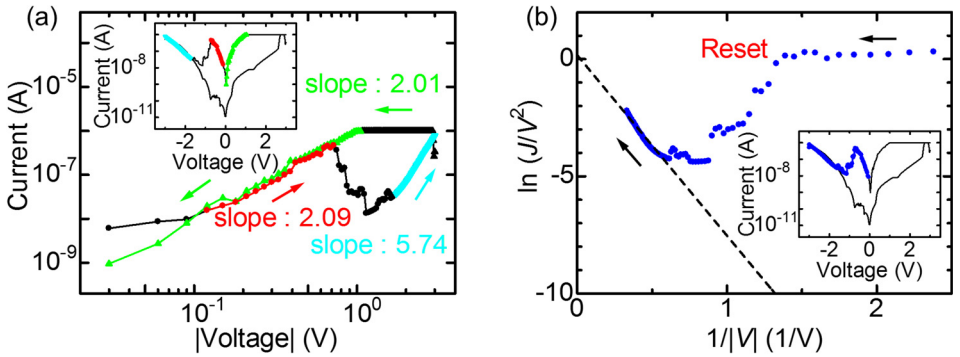

FIG. 5. (a) Double logarithmic plots and (b) Fowler-Nordheim plot of current-voltage characteristics. Arrows show the direction of voltage sweeps.

a Si NC thin film. On the contrary, HRS of current-voltage characteristics is not based on the space charge limited current model because the slope is larger than 2 [Fig. 5(a) and Fig. S4 in the supplementary material). From these results, we conclude that the space charge limited current does not dominate the transport in HRS.

Figure 5(b) shows a Fowler-Nordheim plot of the current-voltage characteristics. The Fowler-Nordheim tunneling model is described as[38]

$$|J| \propto |V|^2 \exp\left(-\frac{1}{|V|}\right), \tag{1}$$

where J and V denote a current density and an applied voltage, respectively. As shown in Fig. 5(b) and Fig. S5 in the supplementary material, negative linear slopes are observed in the high voltage range (>1 V) in HRS. This indicates that the Fowler-Nordheim tunneling process contributes to the current transport in the high voltage range in HRS. It is very plausible that non-stoichiometric SiO_x shells act as tunneling barriers for the charge transport.[22]

By taking into account all the results, the possible switching mechanism of a solution-processed Si NC thin film is schematically proposed in Fig. 6. Initially, oxygen vacancies are distributed in the non-stoichiometric SiO_x shell and thus the resistance of the film is HRS. When V_{Set} is applied to the top electrode, oxygen vacancies in the non-stoichiometric SiO_x are rearranged within a surface of Si NCs by the electric field. Then, a conductive filament of oxygen vacancies is formed. According to Kröger-Vink notation[1,39]

$$O_O^{\times} \rightarrow V_O^{\cdot\cdot} + O_i'', \tag{2}$$

$$O_i'' \rightarrow \frac{1}{2}O_2 + 2e^-, \tag{3}$$

where $O_O^{\times}$ and $V_O^{\cdot\cdot}$ denote an oxygen atom and an oxygen vacancy with +2 charges on a regular site, respectively. O_i'' represents an oxygen ion with −2 charges on an interstitial site. Because the single bond of Si-O has the polarity, the bond is forced by the electric field and it is broken under a strong electric field to form an oxygen vacancy and an oxygen ion.[40] This soft breakdown state is LRS. When V_{Reset} is applied, an opposite electric field diffuses oxygen vacancies from the conductive filament; i.e., oxygen ions compensate oxygen vacancies in the non-stoichiometric SiO_x shell as shown in Fig. 6. This destructs the conductive filament and the resistance returns to HRS. Since the diffusion of oxygen vacancies is induced by the electric field, the solution-processed Si NC thin film shows a bipolar resistive switching [Fig. 2(a)]. It is noted that the total amount of oxygen vacancies does not change during the switching cycles; otherwise, the reproducible switching cannot be observed. We consider that the filament of oxygen vacancies is mainly formed along the surface of the silicon oxide shell because the hysteresis of the resistive switching disappears in oxygen gas. In oxygen gas ambient, oxygen vacancies on the surface are filled with oxygen molecules, and thus, it is difficult to form the filament of oxygen vacancies. However, in this study, we have no clear evidence whether the current flows through only the surface of the oxide shell or both the core and the surface of Si NCs.

In order to further investigate the switching mechanism, the Al top electrode is replaced with a Ag top electrode (Fig. S6). The device with the Ag top electrode and an ITO bottom electrode shows a similar hysteresis curve in current-voltage characteristics. This indicates that the origin of the hysteresis

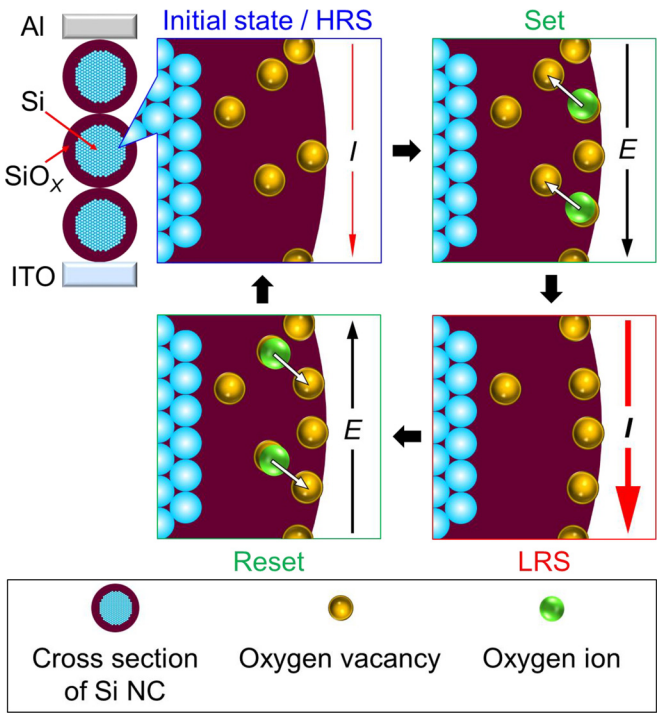

FIG. 6. Possible resistive switching mechanism in a solution-processed Si NC thin film. Formation and destruction of a conductive filament of oxygen vacancies on a non-stoichiometric SiO_x shell are shown.

curve is a Si NC film. However, the device requires a forming process. Resistances of LRS (57 Ω) and HRS (2.6 MΩ) using the Ag top electrode are lower than that of the Al top electrode (LRS: 2.0 MΩ, HRS: 1.4 GΩ). Although a similar hysteresis curve is observed, a forming-free resistive switching does not occur in the device using Ag. By now, we do not have a clear explanation of this dependence of a metal top electrode.

IV. CONCLUSION

In summary, we gave a proof-of-concept to obtain a Si-based and forming-free resistive switching by using a colloidal Si NC solution. The spin-coated Si NC thin film showed forming-free bipolar resistive switching. The resistive switching had a 700 ON/OFF ratio and retained a resistive state for 7000 s. Considering the electrical characteristics at low temperatures and in various gas environments, we proposed that the origin of the resistive switching was the formation and destruction of the conductive filament of oxygen vacancies on a non-stoichiometric SiO_x shell on Si NCs.

SUPPLEMENTARY MATERIAL

See supplementary material for estimation of the thickness of a Si NC thin film, size distribution of colloidal Si NCs, histogram of the height from the AFM image in Fig. 1(e), double logarithmic plots and Fowler-Nordheim plots of current-voltage characteristics, XPS spectrum of an annealed Si NC thin film, and device with a Ag electrode.

ACKNOWLEDGMENTS

We thank Dr. H. Sugimoto for TEM observation and analysis of the XPS spectrum. This work was partly supported by JSPS KAKENHI Grant No. 16H03828, Visegrad Group (V4)-Japan Joint Research Project on Advanced Materials "NaMSeN," and Kawanishi Memorial ShinMaywa Education Foundation.

[1]R. Waser and M. Aono, Nat. Mater. **6**, 833 (2007).
[2]R. Waser, R. Dittmann, C. Staikov, and K. Szot, Adv. Mater. **21**, 2632 (2009).
[3]D.-H. Kwon, K. M. Kim, J. H. Jang, J. M. Jeon, M. H. Lee, G. H. Kim, X.-S. Li, G.-S. Park, B. Lee, S. Han, M. Kim, and C. S. Hwang, Nat. Nanotechnol. **5**, 148 (2010).
[4]T. Kazuya, H. Tsuyoshi, N. Tomonobu, and A. Masakazu, Nature **433**, 47 (2005).
[5]B. J. Choi, A. C. Torrezan, K. J. Norris, F. Miao, J. P. Strachan, M. Zhang, D. A. A. Ohlberg, N. P. Kobayashi, J. J. Yang, and R. S. Williams, Nano Lett. **13**, 3213 (2013).
[6]K. C. Chang, T. M. Tsai, T. C. Chang, H. H. Wu, J. H. Chen, Y. E. Syu, G. W. Chang, T. J. Chu, G. R. Liu, Y. T. Su, M. C. Chen, J. H. Pan, J. Y. Chen, C. W. Tung, H. C. Huang, Y. H. Tai, D. S. Gan, and S. M. Sze, IEEE Electron Device Lett. **34**, 399 (2013).
[7]D. Schmidt, N. Raab, M. Noyong, V. Santhanam, R. Dittmann, and U. Simon, Nanomaterials **7**, 370 (2017).
[8]V. Kannan, Y. S. Chae, C. V. V. Ramana, D. S. Ko, and J. K. Rhee, J. Appl. Phys. **109**, 086103 (2011).
[9]A. Rani, D. B. Velusamy, F. Marques Mota, Y. H. Jang, R. H. Kim, C. Park, and D. H. Kim, Adv. Funct. Mater. **27**, 1604604 (2017).
[10]T. H. Kim, E. Y. Jang, N. J. Lee, D. J. Choi, K. Lee, J. Jang, J. Choi, S. H. Moon, and J. Cheon, Nano Lett. **9**, 2229 (2009).
[11]M. Kim, H. Jung, Y. H. Kim, C. J. Kang, T. S. Yoon, and H. H. Lee, Microelectron. Eng. **136**, 26 (2015).
[12]C. Li, Y. Vaynzof, G. Lakhwani, G. J. Beirne, J. Wang, and N. C. Greenham, J. Appl. Phys. **121**, 144503 (2017).
[13]S. Zhong, S. Duan, and Y. Cui, RSC Adv. **4**, 40924 (2014).
[14]J. Yao, Z. Sun, L. Zhong, D. Natelson, and J. M. Tour, Nano Lett. **10**, 4105 (2010).
[15]A. Mehonic, S. Cueff, M. Wojdak, S. Hudziak, C. Labbé, R. Rizk, and A. J. Kenyon, Nanotechnology **23**, 455201 (2012).
[16]A. Mehonic, S. Cueff, M. I. Wojdak, S. Hudziak, O. Jambois, C. Labbé, B. Garrido, R. Rizk, and A. J. Kenyon, J. Appl. Phys. **111**, 074507 (2012).
[17]A. Mehonic, A. Vrajitoarea, S. Cueff, S. Hudziak, H. Howe, C. Labbé, R. Rizk, M. Pepper, and a. J. Kenyon, Sci. Rep. **3**, 2708 (2013).
[18]A. Mehonic, M. Buckwell, L. Montesi, M. S. Munde, D. Gao, S. Hudziak, R. J. Chater, S. Fearn, D. McPhail, M. Bosman, A. L. Shluger, and A. J. Kenyon, Adv. Mater. **28**, 7549 (2016).
[19]A. Mehonic, T. Gerard, and A. J. Kenyon, Appl. Phys. Lett. **111**, 233502 (2017).
[20]M. Fujii, H. Sugimoto, and K. Imakita, Nanotechnology **27**, 262001 (2016).
[21]H. Sugimoto, M. Fujii, K. Imakita, S. Hayashi, and K. Akamatsu, J. Phys. Chem. C **117**, 11850 (2013).
[22]S. Kano, M. Sasaki, and M. Fujii, J. Appl. Phys. **119**, 215304 (2016).
[23]R. N. Pereira, S. Niesar, W. B. You, A. F. Da Cunha, N. Erhard, A. R. Stegner, H. Wiggers, M. G. Willinger, M. Stutzmann, and M. S. Brandt, J. Phys. Chem. C **115**, 20120 (2011).
[24]R. Gresback, N. J. Kramer, Y. Ding, T. Chen, U. R. Kortshagen, and T. Nozaki, ACS Nano **8**, 5650 (2014).
[25]X. Liu, S. Zhao, W. Gu, Y. Zhang, X. Qiao, Z. Ni, X. Pi, and D. Yang, ACS Appl. Mater. Interfaces **10**, 5959 (2018).
[26]H. Sugimoto, M. Fujii, K. Imakita, S. Hayashi, and K. Akamatsu, J. Phys. Chem. C **117**, 6807 (2013).
[27]H. Sugimoto, M. Fujii, K. Imakita, S. Hayashi, and K. Akamatsu, J. Phys. Chem. C **116**, 17969 (2012).
[28]M. Sasaki, S. Kano, H. Sugimoto, K. Imakita, and M. Fujii, J. Phys. Chem. C **120**, 195 (2016).
[29]S. Kano, K. Kim, and M. Fujii, ACS Sens. **2**, 828 (2017).
[30]R. Alfonsetti, L. Lozzi, M. Passacantando, P. Picozzi, and S. Santucci, Appl. Surf. Sci. **70–71**, 222 (1993).
[31]M. Fujii, H. Sugimoto, M. Hasegawa, and K. Imakita, J. Appl. Phys. **115**, 084301 (2014).
[32]D. Nečas and P. Klapetek, Open Phys. **10**, 181 (2012).
[33]H. Tan, G. Liu, X. Zhu, H. Yang, B. Chen, X. Chen, J. Shang, W. D. Lu, Y. Wu, and R. W. Li, Adv. Mater. **27**, 2797 (2015).
[34]H. Tan, G. Liu, H. Yang, X. Yi, L. Pan, J. Shang, S. Long, M. Liu, Y. Wu, and R. W. Li, ACS Nano **11**, 11298 (2017).
[35]Y. Yang, P. Gao, L. Li, X. Pan, S. Tappertzhofen, S. Choi, R. Waser, I. Valov, and W. D. Lu, Nat. Commun. **5**, 4232 (2014).
[36]T. Tsuruoka, K. Terabe, T. Hasegawa, and M. Aono, Nanotechnology **21**, 425205 (2010).
[37]G. T. Wright, Nature **182**, 1296 (1958).
[38]M. Lenzlinger and E. H. Snow, J. Appl. Phys. **40**, 278 (1969).
[39]J. Chen, C. Hsin, C.-W. Huang, C. Chiu, Y. Huang, S.-J. Lin, W.-W. Wu, and L.-J. Chen, Nano Lett. **13**, 3671 (2013).
[40]J. W. McPherson and H. C. Mogul, J. Appl. Phys. **84**, 1513 (1998).